FERMILAB-CONF-17-554-E-PPD
ACCEPTED

Prepared for submission to JINST

13TH The International Conference "Instrumentation for Colliding Beam Physics" (INSTR-17) from 27 February 2017 to 3 March 2017

Budker Institute of Nuclear Physics (BINP) and Novosibirsk State University (NSU), Novosibirsk, Russia

The Fermilab Muon g-2 experiment: laser calibration system

M. Karuza,[a,b,1] **A. Anastasi**[c,e] **A. Basti**[l] **F. Bedeschi**[l] **M. Bartolini**[l] **G. Cantatore**[b,h] **D. Cauz**[b] **G. Corradi**[c] **S. Dabagov**[c,p,q] **G. Di Sciascio**[g] **R. Di Stefano**[k,f] **A. Driutti**[b] **O. Escalante**[i] **C. Ferrari**[c,d] **A. Fioretti**[c,d] **C. Gabbanini**[c,d] **A. Gioiosa**[n] **D. Hampai**[c] **M. Iacovacci**[f,i] **A. Liedl**[c] **A. Lusiani**[l,m] **F. Marignetti**[k,f] **S. Mastroianni**[f] **D. Moricciani**[g] **G. Pauletta**[b,j] **G.M. Piacentino**[n,o] **N. Raha**[g] **E. Rossi**[c] **L. Santi**[b] **G. Venanzoni**[l] **and the Muon g-2 collaboration**

[a] *University of Rijeka, Rijeka, Croatia*
[b] *INFN, Sezione di Trieste e G.C. di Udine, Trieste, Italy*
[c] *Laboratori Nazionali Frascati dell' INFN, Frascati, Italy*
[d] *Istituto Nazionale di Ottica del C.N.R., UOS Pisa, Pisa, Italy*
[e] *Università di Messina, Messina, Italy*
[f] *INFN, Sezione di Napoli, Napoli, Italy*
[g] *INFN, Sezione di Roma Tor Vergata, Roma, Italy*
[h] *Università di Trieste, Trieste, Italy*
[i] *Università di Napoli, Napoli, Italy*
[j] *Università di Udine, Udine, Italy*
[k] *Università di Cassino, Cassino, Italy*
[l] *INFN, Sezione di Pisa, Pisa, Italy*
[m] *Scuola Normale Superiore, Pisa, Italy*
[n] *INFN, Sezione di Lecce, Lecce, Italy*
[o] *Università del Molise, Pesche, Italy*
[p] *PN Lebedev Physical Institute, Moscow, Russia*
[q] *NR Nuclear University MEPhI MEPhI, Moscow, Russia*

E-mail: mkaruza@phy.uniri.hr

[1] Corresponding author.

This document was prepared by Muon G-2 collaboration using the resources of the Fermi National Accelerator Laboratory (Fermilab), a U.S. Department of Energy, Office of Science, HEP User Facility. Fermilab is managed by Fermi Research Alliance, LLC (FRA), acting under Contract No. DE-AC02-07CH11359.

Abstract: The anomalous muon dipole magnetic moment can be measured (and calculated) with great precision thus providing insight on the Standard Model and new physics. Currently an experiment is under construction at Fermilab (USA) which is expected to measure the anomalous muon dipole magnetic moment with unprecedented precision. One of the improvements with respect to the previous experiments is expected to come from the laser calibration system which has been designed and constructed by the Italian part of the collaboration (INFN). An emphasis of this paper will be on the calibration system that is in the final stages of construction as well as the experiment which is expected to start data taking this year.

Keywords: Cherenkov detectors, lasers, optics, Detector alignment and calibration methods

Contents

1 Introduction

1.1 Theory

The Fermilab Muon g-2 experiment continues a series of measurements of the muon's magnetic dipole moment and can be considered as an upgraded version of Brookhaven E821 Experiment with whom it shares the muon storage ring. The physics involved in the experiment is in the first approximation fairly simple. It is based on the behaviour of a charged particle, in this case an anti-muon, with a non zero magnetic dipole moment in a magnetic field. A positively charged particle moving with a velocity v in a magnetic field will be subjected to Lorentz force which will curve its trajectory and in a right combination of the field's intensity and geometry it will move in circles with cyclotron frequency $\omega_c = \frac{e \cdot B}{m\gamma}$. Since the particle has a non zero magnetic dipole moment $\vec{\mu}$ it will also experience a torque $\tau = \vec{\mu} \times \vec{B}$ that tends to align it with the magnetic field lines. In case the particle also spins around its axis which is parallel to its velocity vector and dipole moment, it will precess in the direction given by the torque vector with frequency

$$\omega_s = \frac{geB}{2m} + (1 - \gamma)\frac{eB}{m\gamma} \tag{1.1}$$

where g is muon g-factor, a proportionality constant that relates the observed magnetic moment μ of a particle to its spin angular momentum. The second member in the equation is the relativistic correction to spin precession frequency the Thomas precession [1]. It can be immediately verified from Eq. (1.1) that in the case when $g = 2$, which is expected from quantum mechanics, the difference between spin precession and cyclotron frequency $\omega_a = \omega_s - \omega_c$ is equal to zero. In the anti-muon case g-factor differs from 2 and $\omega_a \neq 0$. The experimentally measured value is the anomalous precession frequency ω_a, which, if the magnetic field is known, gives us the g-2 value; the so called anomalous magnetic moment a_μ. Unfortunately the experimental setup includes also electric fields needed for the containment of anti-muons in their orbits since their transverse

momentum in the instant they enter the storage ring is not exactly zero. This electric field in the anti-muons rest frame becomes a magnetic field in the laboratory frame and contributes to the overall precession with an additional factor which vanishes at so called "magic momentum", at $\gamma = 29.38$. In these conditions the anomalous precession frequency ω_a depends only on the magnetic field B as in the Equation 1.1. The reason why the g-factor differs from two can be found in quantum physics where, besides the basic Feynman diagram which describes the interaction of the charged particle with an external magnetic field, there are several diagrams including QED, electroweak (EW) and strong interactions [2]. Today, thanks to various experimental efforts and advances in theory, the contribution of different diagrams foreseen by the Standard Model can be calculated.

$$a_\mu^{SM} = a_\mu^{QED} + a_\mu^{EW} + a_\mu^{Had} \tag{1.2}$$

The largest contribution comes from the QED part which considers interactions with photons and leptons; the EW part includes interactions with heavier particles such as W^{+-}, Z and Higgs, while the hadronic part considers strong interaction, i.e. diagrams with quarks and gluons. The last one can be further separated in lowest order (LO) and higher order hadronic vacuum polarization contributions (NLO). The calculated values foreseen by the Standard Model (SM) are given in the following table [2], as well as current experimental result.

CONTRIBUTION	RESULT in 10^{-11}
QED	116 584 718.95(0.08)
EW	153.6(1.0)
HAD(LO)	6923(42)
HAD(NLO)	7(26)
Theory	116 591 803 (1)(42)(26)
Experiment	116 592 091(54)(33)
Difference	288 (63)(49)

Table 1. Contribution of various interactions to magnetic moment anomaly. Errors are given in parenthesis. In the difference the errors coming from theory and experiment are summed in quadrature.

It is evident, from the results shown in Table 2 , that there is 3.5 σ discrepancy between the SM predicted and last experimentally obtained value. The goal of the E989 experiment and the Muon g-2 collaboration is to reduce the experimental errors and by doing it remove or confirm this discrepancy. In case the discrepancy is confirmed it will give a confirmation that new physics beyond the SM exists, unfortunately without explaining its nature.

1.2 Experiment

After it became clear that the experiment will be made at Fermilab, the question about the muon storage ring was raised. The options were either construct a new one or reuse the Brookhaven one. The choice fell on using the Brookhaven one since it behaved very well in the experiment and no further improvement was expected by building a new one, while moving it would save fair amount of money. In summer 2013 the ring started its voyage from Brookhaven to Batavia by circumnavigating Florida, following upstream Mississipi and Illinois rivers it arrived close to the Fermilab National

Laboratory. The last, approximately 50 kilometers long, part of the trip was made on road during three nights. This was only a first step in building the experiment. The next step was to reassemble the magnets and place 700 tons of steel in a temperature controlled environment, with excursion lower than one degree celsius with 125 micron tolerance. The pole pieces of the g-2 Lambertson magnet had to be aligned to 25 micron. After all the pieces where in place the magnet was powered up and full power was achieved on September 21st 2015. At this moment the fine tuning could start. Ideally the magnetic field should be uniform in the ring, however there were some variations at the 1400 ppm level that had to be corrected. This was done by shimming with the goal of 50 ppm which gives a muon weighted systematic uncertainty of 70 ppb, a factor 2 improvement over previous experiment. At the end of January 2017 all the pieces of the experiment were in place and ready for the commissioning as it was foreseen in the schedule. When systematic errors related to the magnetic field measurements have been minimised, the only other quantity to be measured is the anomalous precession frequency ω_a and also in this measurements the systematic uncertainties have to be handled. The comparison between Brookhaven and Fermilab projected uncertainties [3] are given in the following table. The first two entries are directly related to the calorimeters used

CATEGORY	Brookhaven (ppb)	Fermilab	Goal (ppb)
Gain changes	120	Better laser calibration, low energy threshold	20
Pileup	80	Low energy samples recorded, calorimeter segmentation	40
Lost muons	90	Better collimation in ring	20
Coherent betatron oscillation	50	Higher n value (frequency), Better match of beamline to ring	<30
E and pitch	50	Improved tracker, Precise storage ring simulations	30
Total	180	Quadrature sum	70

Table 2. Contribution of various processes to magnetic moment anomaly.

for positron detection and the biggest contribution in reducing the systematic error is expected in this field. This will be done by using a new improved laser calibration system (LCS) to calibrate the response of the calorimeters to the physical signal. Bear in mind that 24 calorimeters distributed around the muon storage ring consist of 54 crystals each which gives a total of approximately 1300 channels. Each of this channels has a dedicated detector, a SiPM in this case, whose photon detection efficiency has to be known. This is of utmost importance since the energy of the positrons in the laboratory frame can be associated with the anti-muon spin direction in the moment of the decay. The high energy positrons are emitted when the spin is parallel to the momentum while low energy positrons are emitted when the spin is antiparallel to the momentum. The spectrum [3] as a function of time is shown in Fig. 1

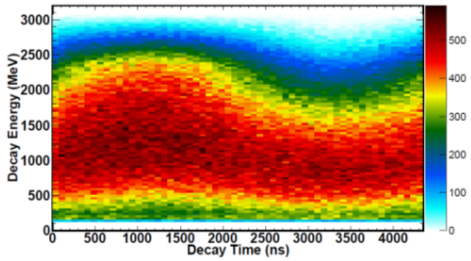

Figure 1. The decay positron energy spectrum. The difference between aligned (1090 ns) and anti-aligned (3271 ns) anti-muon spin and momentum is prominent for energies greater than 1800 MeV.

2 Light calibration system

The LCS consists of four main subsystems, the light source, the distribution system [5], source monitor (SM) [4] and local monitor (LM) [6]. While the source, SM and LM are placed inside a dedicated room called Laser hut outside the ring, the majority of the distribution systems is attached to the calorimeters placed inside the muon storage ring. The light is sent between the laser hut and the ring by 25 m long quartz optical fibers.

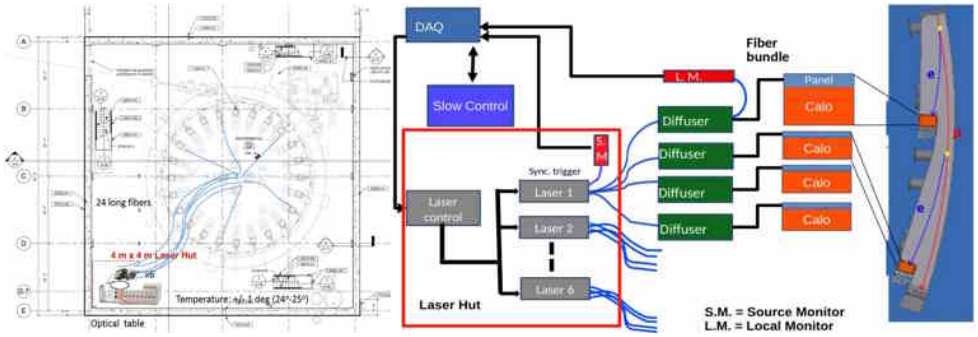

Figure 2. Schematic drawing of the experimental hall with the position of the muon storage ring and laser hut (left). The LCS scheme can be seen on the right.

2.1 Local and source monitor

The intensity variations of the light source used for calibration are monitored by the so called source monitor (SM) while the intensity variations in the light distribution are monitored by the local monitor (LM). The light source consists of six LDH-P-C-405 M Picoquant laser heads driven with single Sepia II 828 controller. The light from each laser is divided with unbalanced beamsplitter in two (70-30) where the lower intensity beam goes to the SM. The SM consists of a commercial integrating sphere (Thorlabs IS200) equipped with two large area (10 mm x 10 mm) photodiodes (Hamamatsu S3590-18), one PMT (Hamamatsu H5783) and a low activity (6 Hz) Am source coupled to NaI crystal which illuminates the PMT thus providing an absolute calibration reference. To one of the integrating sphere's ports a mini-bundle is attached which consists of ten, 3 m long fibers that take light signal to the LM PMTs. This direct signal is compared in the LM with the delayed signal that has made a roundtrip to the calorimeters. The higher intensity beam coming

from the beamsplitter passes through a filter, placed in a filter wheel which is used to adjust the light intensity, and afterwards is divided by a series of 50:50 beamsplitters in four equal beams that serve four different calorimeter stations. For the SM a custom made electronics has been made which is integrated with the optics and detectors. Everything is placed in an aluminum housing thus providing a large thermal inertia.

2.2 Distribution

The light enters the outgoing optical fiber through an adjustable collimator and arrives to the calorimeter station after 25 m. At the calorimeter station the fibers enters in light distribution box where the light exits the fiber and then goes through a collimation lens and an engineered diffuser (Thorlabs ED-20) which tailors the light intensity from the fiber to a flat top profile. Only now the light illuminates a bundle, with 54 one meter long fibers, that connects the distribution box to light distribution plate. The plate is made of 1 cm thick plastic material (Delrin) and is placed in front of the calorimeter crystals. It not only provides the calibration signal, but also holds the crystals in place from the front side. Each plate was milled at LNF mechanical workshop, where channels housing the fibers and rectangular apertures were made. There are, in each plate, in total 54 channels, where fibers were inserted, and apertures where optical prisms, which serve to steer the light at 90 degrees into the calorimeter crystals, are glued. The light coming from the prisms illuminates each of the 54 PbF_2 crystals in every of the 24 calorimeter stations. Moreover, besides the bundle, the diffused light illuminates two more 25 m long fibers, one quartz and the other in PMMA, that are going back to the laser hut where the LM is placed.

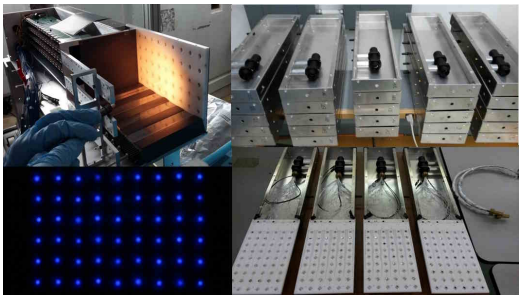

Figure 3. Photos from the distribution system. Clockwise from top left corner; front panel with prisms is being mounted on the calorimeter, diffuser boxes are waiting for the front panels and optical fibers, diffuser boxes with front panels and fibers in place, blue light coming from a front panel.

2.3 Local monitor

The principal component of the LM is a Photonics XP2982 PMT that receives two laser pulses. The first one is a reference signal from the SM, while the other is coming from the calorimeters placed in the ring and is representative of the calibration signal sent to the calorimeters. The PMT's are contained in custom made cases which hold 10 PMTs and signal conditioning electronics. The light before reaching the photocathodes passes through an interferential bandpass filter centered at 405 nm, with 10 nm halfwidth, which filters out possible background light coming from other sources than LCS. The two signals, which are derived from the same laser pulse are separated about 250 ns

(Fig. 4) since one is arriving directly from the laser through SM and 2 m long minibundle fibers, and the other makes a 50 m long roundtrip to the calorimeters and back.

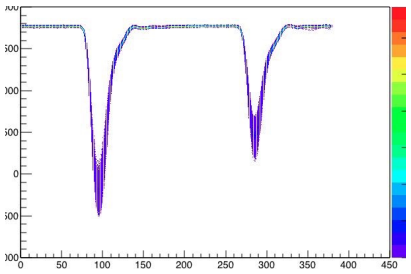

Figure 4. Persistance plot of a LM PMT signal. Commissioning run with 2600 events.

Two pulses can be directly compared since the expected gain fluctuations of a PMT at this timescale are negligible. In order to study and compensate for any fluctuations due to temperature of the transmission coefficient of the local monitor optical fibers, we will use two types of fibers: quartz and PMMA. The system is redundant, and allows to monitor any solarizing effect of the PMMA fibers.

3 Conclusion

The function of the LCS is to provide calibration pulses for the detectors that closely simulate the physics signals expected from the positron interaction with the calorimeter crystals. In order to achieve the desired precision a novel setup has been designed and constructed in Italy and assembled at Fermilab. The tests have shown the feasibility of a stabilization at the level of 10^{-4} per hour.

Acknowledgments

This research was supported by Istituto Nazionale di Fisica Nucleare (Italy) and by the EU Horizon 2020 Researchand Innovation Programme under the Marie Sklodowska-Curie Grant Agreement No. 690835. SD would like to thank the support by the Competitiveness Program of National Research Nuclear University MEPhI.

References

[1] Thomas, L. H., *The Motion of the Spinning Electron*, *Nature* **117** (1926) pg.514.

[2] C. Patrignani et al. (Particle Data Group), *Review of Particle Physics*, *C*hin. Phys. C, **40** (2014) pg. 635

[3] J. Grange et al., *Muon (g-2) Technical Design Report*, arxiv:1501.06858v1.

[4] A. Anastasi et al., *The calibration system of the new g − 2 experiment at Fermilab*, *N*IM A, **824** (2016) pg. 716

[5] A. Anastasi et al., *Test of candidate light distributors for the muon (g-2) laser calibration system*, *N*IM A, **788** (2015) pg. 43

[6] A. Anastasi et al., *Electron beam test of key elements of the laser-based calibration system for the muon g-2 experiment*, *N*IM A, **842** (2017) pg. 86